Approximate calculation of femtosecond pump–probe spectra monitoring nonadiabatic excited-state dynamics

Stefan Dilthey, Susanne Hahn, and Gerhard Stock

Citation: The Journal of Chemical Physics **112**, 4910 (2000); doi: 10.1063/1.481045
View online: http://dx.doi.org/10.1063/1.481045
View Table of Contents: http://scitation.aip.org/content/aip/journal/jcp/112/11?ver=pdfcov
Published by the AIP Publishing

Approximate calculation of femtosecond pump–probe spectra monitoring nonadiabatic excited-state dynamics

Stefan Dilthey, Susanne Hahn, and Gerhard Stock[a)]
Theoretical Quantum Dynamics, Faculty of Physics, University Freiburg, D-79104 Freiburg, Germany

(Received 21 October 1999; accepted 16 December 1999)

An approximate theory of femtosecond spectroscopy of nonadiabatically coupled electronic states is developed. Neglecting the commutators of vibrational Hamiltonians pertaining to different diabatic electronic states, the formulation represents a generalization of the semiclassical Franck–Condon approximation to the case of nonadiabatic dynamics. Explicit expressions for various time- and frequency-resolved spectra are derived which allow for a simple interpretation of femtosecond spectroscopy of vibronically coupled molecular systems. Employing multidimensional model problems describing (i) the nonadiabatic *cis–trans* isomerization of an electronic two-state system, and (ii) the $S_2 \rightarrow S_1$ internal conversion of pyrazine, exact reference data are compared to approximate calculations of transient absorbance and emission as well as time-resolved photoelectron spectra. In all cases considered, the approximation is shown to be appropriate for probe–pulse durations that are shorter than the period of the fastest relevant vibrational mode of the molecular system. Reducing the numerical costs of pump–probe simulations to the costs of a standard time-dependent wave-packet propagation, the approximate theory leads to substantial computational savings. © *2000 American Institute of Physics.* [S0021-9606(00)01310-6]

I. INTRODUCTION

Over the last 20 years, the time-dependent formulation of optical spectroscopy has become quite popular in chemical physics.[1] The approach may result in considerable computational savings, facilitates the use of various approximations, and offers an appealing interpretation of spectroscopic processes. For example, consider the general expression for the linear continuous wave (cw) absorption spectrum[2]

$$\sigma_A(\omega) = \int \mathrm{d}t\, e^{i\omega t} \langle \phi | \mu_{12} e^{-ih_2 t} \mu_{21} e^{ih_1 t} | \phi \rangle. \tag{1.1}$$

In the case of electronic spectroscopy, $|\phi\rangle$ denotes the initial vibrational state of the system, $h_n = T + V_n$ represents the vibrational Hamiltonian pertaining to the nth electronic state ($n = 1,2$), and μ_{12} is the dipole moment of the electronic transition. Throughout this work we set $\hbar = 1$. Equation (1.1) can be interpreted as follows: Upon absorption of a photon with frequency ω, the ground-state wave function $e^{ih_1 t}|\phi\rangle$ is lifted on the excited-state potential-energy surface V_2, thus resulting in the nonstationary state $|\Psi(t)\rangle = e^{-ih_2 t}\mu_{21} e^{ih_1 t}|\phi\rangle$. The absorption spectrum can therefore be rationalized via the time evolution of the excited-state wave packet $|\Psi(t)\rangle$ projected onto its initial state $|\Psi(0)\rangle$, thus providing a dynamical interpretation of the cw spectrum.[3]

Let us now assume that the Condon approximation holds (i.e., that the transition dipole moment μ_{nm} is coordinate independent) and that the time-dependent overlap $\langle \Psi(0)|\Psi(t)\rangle$ decays rapidly, e.g., as it is the case for direct photodissociation. This allows us to employ the short-time approximation $e^{-ih_2 t} e^{ih_1 t} \approx e^{-i(V_2 - V_1)t}$, which results in a particularly simple picture of the absorption process: The spectrum $\sigma_A(\omega)$ is essentially determined by the resonance condition $\omega = V_2 - V_1$, where $V_2 - V_1$ is the electronic energy gap in the Franck–Condon region.[1,4–6] Since the short-time assumption becomes exact in the classical limit, this ansatz is sometimes referred to as semiclassical Franck–Condon approximation.[4] In the context of direct photodissociation, the approximation has also been referred to as the ''reflection principle.''[5]

A time-dependent description appears to be particularly natural for the modeling of *time-resolved* experiments, which aim to observe the dynamics of molecular processes in real time.[7–9] Most of these experiments are of the pump–probe type; that is, the molecular system is prepared at time $t = 0$ by a first laser pulse (the ''pump'') into a nonstationary state $|\Psi_0\rangle$, whose time evolution is interrogated by a second laser pulse (the ''probe'') at the delay time t_d. To be specific, let us furthermore assume (i) that the excitation is resonant, thus resulting in a population of the excited state, (ii) that the pump and probe pulses do not overlap, thus facilitating the interpretation of signals, and (iii) that there only is a single probe process, e.g., stimulated emission into the electronic ground state. As is shown below, the pump–probe signal can then be written as

$$I(t_d) = \langle \Psi_0(t_d) | P^\dagger P | \Psi_0(t_d) \rangle, \tag{1.2}$$

where the time-dependent excited-state wave function $|\Psi_0(t_d)\rangle$ depends on its preparation by the pump pulse and the stimulated-emission projection operator P incorporates the action of the probe pulse.

Assuming short probe pulses, we may evaluate the pump–probe signal within the semiclassical Franck–Condon

a)Electronic mail: stock@physik.uni-freiburg.de

approximation.[1,10–16] This leads to a *time-dependent* resonance condition $\omega = V_2(t_d) - V_1(t_d)$, where ω is the carrier frequency of the probe pulse and the time dependency of the electronic energy gap is due to the fact that the electronic transition occurs at the instantaneous position of the vibrational wave packet $|\Psi_0(t_d)\rangle$. The semiclassical Franck–Condon approximation therefore leads to the physically appealing picture that a pump–probe experiment monitors the time-dependent Franck–Condon overlap between the prepared nonstationary state and the projector state, whereby the probe laser frequency is chosen to match the instantaneous electronic energy gap. Apart from interpretative purposes, the approximation may also help to considerably reduce the computational effort of a pump–probe simulation. Employing a suitable (e.g., Gaussian) form of the electric field, the ansatz allows for an analytical evaluation of the time integration in P, and also leads to a particularly simple treatment of continuum states.[10–12]

In many cases, however, the theoretical description of photoinduced molecular dynamics is complicated by the fact that the underlying Born–Oppenheimer assumption of noninteracting adiabatic potential-energy surfaces may break down. Numerous experimental and theoretical investigations have indeed revealed that (avoided or real) crossings of adiabatic potential-energy surfaces represent the rule rather than the exception in polyatomic systems.[17–19] To account for this situation, multidimensional time-dependent wave-packet calculations on coupled potential-energy surfaces,[5,19–21] as well as simulations of the corresponding femtosecond time- and frequency-resolved spectra,[19,22–25] have been reported. While the numerically exact calculation of nonadiabatic dynamics and spectra is (at least in principle) straightforward, the calculation of electronic spectra within the semiclassical Franck–Condon approximation is *a priori* not clear, since the very concept of this approximation is based on the Born–Oppenheimer picture.

In this paper we extend the theoretical description of time- and frequency-resolved spectra within the semiclassical Franck–Condon approximation to the case of nonadiabatically coupled potential-energy surfaces. Two qualitatively different cases may occur: intramolecular and radiative couplings pertain to (a) the *same* electronic transition, and (b) to *different* electronic transitions. The two different situations are illustrated in Fig. 1, which schematically shows two molecular models with coupled electronic states $|\psi_1\rangle$ and $|\psi_2\rangle$. In case (a), referred to as the ''internal transition'' case, the radiation field induces transitions between the two vibronically coupled states $|\psi_1\rangle$ and $|\psi_2\rangle$. In case (b), referred to as the ''external transition'' case, one considers radiative transitions from the coupled states $|\psi_1\rangle$, $|\psi_2\rangle$ to one (or several) additional ''detector state(s)'' $|\psi_d\rangle$. This may be achieved via emission into the electronic ground state, by absorption into an excited electronic state, and through the ionization of the molecule.

In both cases, we develop a comprehensive theory of pump–probe spectroscopy which is shown to lead to a natural extension of the Born–Oppenheimer picture. We derive explicit expressions for various transient signals, thereby obtaining a simple interpretation of femtosecond spectroscopy

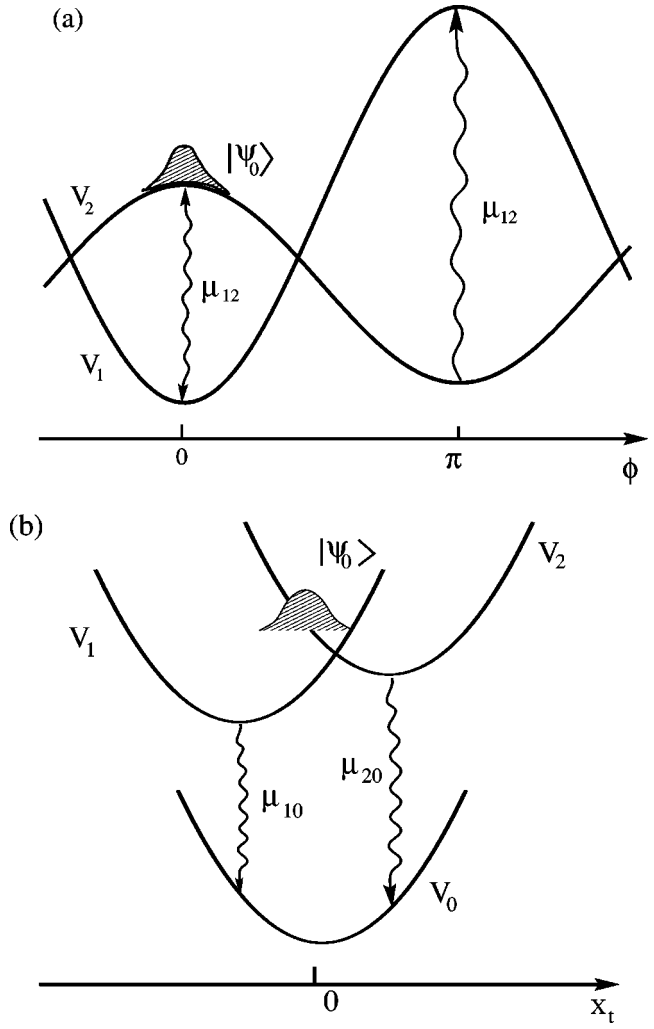

FIG. 1. Schematic view of the diabatic potential-energy curves V_n for various model problems of vibronic coupling. At time $t=0$, the system is prepared by an impulsive pump pulse into a nonstationary state $|\Psi_0\rangle$, whose time evolution is interrogated by a time-delayed probe pulse which may induce internal or external electronic transitions. (a) Internal case, i.e., the radiation field induces transitions between the two coupled electronic states. Shown are the torsional potentials of a three-mode model describing nonadiabatic *cis–trans* photoisomerization (Ref. 24). (b) External case, i.e., the radiation field induces transitions from the coupled states to an additional detector state with potential V_0. Shown are the potential curves along a totally symmetric mode of a three-mode model describing the $S_2 \rightarrow S_1$ internal conversion in pyrazine (Ref. 26).

of nonadiabatically coupled molecular systems. Employing multidimensional model problems describing (i) the nonadiabatic *cis–trans* isomerization of an electronic two-state system,[24] and (ii) the $S_2 \rightarrow S_1$ internal conversion of pyrazine,[26] we compare approximate calculations of various femtosecond spectra to exact reference data. In all cases considered, the approximate theory is shown to be excellent for short enough probe-pulse durations, while the computational effort is reduced significantly.

II. THEORY

A. Model and spectroscopic signals

A curve-crossing problem can be formulated in the adiabatic as well as in a diabatic electronic representation, both

having well-known advantages and shortcomings. Adiabatic electronic wave functions and the corresponding Born–Oppenheimer potential-energy surfaces are the familiar output of standard electronic structure calculations. Furthermore, the interpretation of nonadiabatic relaxation processes appears to be most straightforward in the adiabatic representation. In many cases of interest, however, a *diabatic* representation exhibits more clearly the basic physics occurring on intersecting potential-energy surfaces. This is because diabatic potential-energy surfaces can often be modeled in terms of a low-order Taylor expansion, whereas the shape of the adiabatic potential-energy surfaces may be rather complicated and thus defies a low-order polynomial representation. Furthermore, transitions between diabatic electronic states are important for the interpretation of spectroscopic data, since in the vicinity of surface crossings the electronic transition dipole operator is only smooth in the diabatic representation. Employing both the adiabatic and the diabatic representation, in the following we introduce the model Hamiltonian and spectroscopic signals under consideration. For further information on general concepts of non-Born–Oppenheimer dynamics, we refer to Refs. 17–20.

1. Hamiltonian

Adopting a diabatic electronic representation, the molecular model Hamiltonian can be written as[20]

$$H=\sum_n |\psi_n\rangle h_n\langle\psi_n| + \sum_{n\neq m} |\psi_n\rangle V_{nm}(x)\langle\psi_m|, \tag{2.1}$$

comprising the vibrational Hamiltonian $h_n=T+V_n(x)$ in the diabatic electronic state $|\psi_n\rangle$ and the off-diagonal diabatic coupling elements $V_{nm}(x)$. In this work we focus on the simplest case that only two electronic states are nonadiabatically coupled, resulting in

$$H=h\mathbb{1}+\Delta\sigma_z+V\sigma_x, \tag{2.2}$$

where $h=T+\frac{1}{2}(V_1+V_2)$, $\Delta=\frac{1}{2}(V_2-V_1)$, and $V=V_{12}=V_{21}$. For convenient notation, Pauli matrices σ_x, σ_y, σ_z, and the unit matrix $\mathbb{1}$ have been introduced.

Employing a unitary transformation S that diagonalizes the diabatic potential matrix, the molecular Hamiltonian in the adiabatic representation can be written as

$$H_{\mathrm{ad}}=S^{\dagger}HS=\sum_n |\psi_n^{\mathrm{ad}}\rangle[T+W_n(x)]\langle\psi_n^{\mathrm{ad}}| + \Lambda, \tag{2.3}$$

where we have introduced adiabatic basis states $|\psi_n^{\mathrm{ad}}\rangle$ and adiabatic potential-energy surfaces $W_n(x)$. The non-Born–Oppenheimer operator Λ is responsible for nonadiabatic transitions of the molecule, i.e., $\Lambda=0$ corresponds to the Born–Oppenheimer approximation.

For the two-state problem (2.2), the adiabatic potential-energy surfaces $W_n(x)$ as well as the unitary transformation S can be expressed in closed form[20]

$$W_1=\tfrac{1}{2}(V_1+V_2)-W, \tag{2.4a}$$

$$W_2=\tfrac{1}{2}(V_1+V_2)+W, \tag{2.4b}$$

$$S_{11}=S_{22}=\sqrt{\frac{1}{2}\left(1+\frac{\Delta}{W}\right)}, \tag{2.5a}$$

$$S_{12}=-S_{21}=\sqrt{\frac{1}{2}\left(1-\frac{\Delta}{W}\right)}, \tag{2.5b}$$

where $W=\sqrt{\Delta^2+V^2}$.

Apart from the molecular Hamiltonian, the field–matter interaction $H_{\mathrm{int}}(t)$ needs to be specified to describe a spectroscopic experiment. Within the electric dipole approximation, the interaction between the molecular system and the external electric field $\mathcal{E}(t)$ is given by

$$H_{\mathrm{int}}(t)=-\hat{\mu}\mathcal{E}(t). \tag{2.6}$$

The transition dipole operator

$$\hat{\mu}=\sum_{n\neq m} |\psi_n\rangle\mu_{nm}\langle\psi_m| \tag{2.7}$$

is defined in the diabatic representation. As explained above, this ensures that the matrix elements μ_{nm} are only weakly dependent on nuclear coordinates, i.e., that the Condon approximation is valid.

Let us finally consider the case that the vibronically coupled system is probed via time-resolved ionization. Apart from the N-state system (2.1), the total molecular Hamiltonian H_t then contains a term describing the ionization continuum

$$H_t=H+\sum_n \int_0^{\infty} \mathrm{d}E_k |\psi_n^{(k)}\rangle(\tilde{h}_n+E_k)\langle\psi_n^{(k)}|, \tag{2.8}$$

where $\tilde{h}_n=T+\tilde{V}_n(x)$ represents the vibrational Hamiltonian of the ionic state $|\psi_n^{(k)}\rangle$ and the index k labels the energy E_k of the continuum electrons. The corresponding transition dipole operator reads

$$\hat{\mu}=\sum_{n,m} \int_0^{\infty} \mathrm{d}E_k |\psi_n^{(k)}\rangle\mu_{nm}(E_k)\langle\psi_m| + \mathrm{h.c.} \tag{2.9}$$

2. Spectroscopic signals

Assuming that at time $t=0$ the molecular system has been excited by an impulsive pump pulse, we focus on the interaction of the prepared nonstationary state $|\Psi_0(t)\rangle$ with the probe pulse. The extension of the theory to the case of finite pump pulses and overlapping laser fields is discussed in Sec. III D. The probe pulse is given by

$$\mathcal{E}(t)=\mathcal{E}_0 e^{-(t-t_d)^2/(4\alpha\tau^2)} e^{-i\omega(t-t_d)} + \mathrm{c.c.}, \tag{2.10}$$

where the probe field $\mathcal{E}(t)$ is characterized by its carrier frequency ω, the pulse duration (FWHM) τ, and the delay time t_d. The amplitude $\mathcal{E}_0$ is chosen to fulfill the normalization condition $\int \mathrm{d}t\, \mathcal{E}(t)=1$, and $1/\alpha=16\ln 2$.

Employing time-dependent perturbation theory with respect to the field–matter interaction, the wave function after the interaction with the probe field can be written as

$$\begin{aligned}|\Psi_P(t)\rangle &= i\int_{-\infty}^{\infty} \mathrm{d}t'\, \mathcal{E}(t') e^{-iH(t-t')}\hat{\mu}|\Psi_0(t')\rangle \\ &= ie^{-iH(t-t_d)}\int_{-\infty}^{\infty} \mathrm{d}t'\, \mathcal{E}(t') e^{-iH(t_d-t')}\hat{\mu} \\ &\quad \times e^{iH(t_d-t')}|\Psi_0(t_d)\rangle,\end{aligned} \tag{2.11}$$

where $|\Psi_0(t)\rangle$ denotes the nonstationary state prepared by the pump pulse and t_d denotes the delay time between the two pulses. In what follows, it is convenient to rewrite Eq. (2.11) as

$$|\Psi_P(t_d)\rangle = P|\Psi_0(t_d)\rangle, \tag{2.12}$$

$$P = i\int_{-\infty}^{\infty} dt'\ \mathcal{E}(t')e^{-iH(t_d-t')}\hat{\mu}e^{iH(t_d-t')}. \tag{2.13}$$

Note that the propagator P accounts for the field–matter interaction in a perturbative manner, while the (presumably strong) intramolecular interaction is treated to all orders in V.

Assuming that the measured absorption/emission signal is directly proportional to the field-induced population in the final electronic state, the spectroscopic signal is given by

$$I(t_d) = \langle\Psi_P(t_d)|\Psi_P(t_d)\rangle. \tag{2.14}$$

In the case of time-resolved ionization spectroscopy, one may monitor the energy spectrum of the photoelectrons, which is represented by the population probability density of the ionization continua[10,23]

$$I_{\mathrm{Ion}}(E_k,t_d) = \sum_n \langle\Psi_P(t_d)|\psi_n^{(k)}\rangle\langle\psi_n^{(k)}|\Psi_P(t_d)\rangle. \tag{2.15}$$

The total ion yield is then given by

$$I_{\mathrm{Ion}}(t_d) = \int_0^{\infty} dE_k\, I_{\mathrm{Ion}}(E_k,t_d). \tag{2.16}$$

B. Internal transitions

Adopting the diabatic two-state system (2.2), we first consider the case of internal radiative transitions; that is, the radiation field induces transitions between the two vibronically coupled states $|\psi_1\rangle$ and $|\psi_2\rangle$. The transition dipole operator is thus given by

$$\hat{\mu} = \mu\sigma_x = \mu|\psi_1\rangle\langle\psi_2| + \mathrm{h.c.}, \tag{2.17}$$

with $\mu = \mu_{12} = \mu_{21}$. In what follows we wish to evaluate the propagator (2.13) in the spirit of the semiclassical Franck–Condon approximation. The short-time approximation $e^{-ih_2t}e^{ih_1t} \approx e^{-i(h_2-h_1)t}$ inherent to this ansatz can be extended to the case of nonadiabatically coupled electronic states through the following approximations:

$$[h_n,h_m] = 0, \tag{2.18a}$$

$$[h_n,V_{nm}] = 0, \tag{2.18b}$$

i.e., in addition to Eq. (2.18a) we moreover need to assume that the vibronic coupling operators V_{nm} commute with the vibrational Hamiltonians h_n. Since these commutators generally depend on vibrational momenta, this approximation amounts to neglecting the motion of the vibrational wave packet during the probe pulse.[10] Clearly, this assumption can only be valid for sufficiently short probe pulses.

To apply approximation (2.18) to the Heisenberg dipole operator $\hat{\mu}(t) = e^{-iHt}\hat{\mu}e^{iHt}$ occurring in Eq. (2.13), we use the well-known operator expansion

$$e^{-\alpha\hat{A}}\hat{B}e^{\alpha\hat{A}} = \hat{B} - \alpha[\hat{A},\hat{B}] + \frac{\alpha^2}{2!}[\hat{A},[\hat{A},\hat{B}]] - \frac{\alpha^3}{3!}[\hat{A},[\hat{A},[\hat{A},\hat{B}]]] + \ldots \tag{2.19}$$

Employing Eq. (2.18), we obtain for the first terms

$$[H,\hat{\mu}] = -2i\mu\Delta\sigma_y, \tag{2.20a}$$

$$[H,[H,\hat{\mu}]] = 4\mu\Delta(\Delta\sigma_x + V\sigma_z), \tag{2.20b}$$

$$[H,[H,[H,\hat{\mu}]]] = -8i\mu W^2\Delta\sigma_y \tag{2.20c}$$

$$= 4W^2[H,\hat{\mu}], \tag{2.20d}$$

whereby the linear term is exact while higher-order terms are approximate due to (2.18). The infinite sum on the right-hand side of Eq. (2.19) can thus be written in closed form

$$\hat{\mu}(t) = \mu\left\{\sigma_x - \frac{\Delta}{W}\sin(2Wt)\sigma_y + \frac{\Delta}{W}[\cos(2Wt)-1]\left[\frac{\Delta}{W}\sigma_x + \frac{V}{W}\sigma_z\right]\right\}. \tag{2.21}$$

In the absence of vibronic coupling ($V=0$), Eq. (2.21) reduces to the well-known result

$$\hat{\mu}(t) = \mu\{\cos(2\Delta t)\sigma_x - \sin(2\Delta t)\sigma_y\} = \mu e^{-i2\Delta t}|\psi_2\rangle\langle\psi_1| + \mathrm{h.c.} \tag{2.22}$$

The same result can be obtained by direct exponentiation of iHt. Within the approximation (2.18) we obtain

$$e^{\pm iHt} = \left\{\cos(Wt)\mathbb{1} \mp i\sin(Wt)\left(\frac{\Delta}{W}\sigma_z - \frac{V}{W}\sigma_x\right)\right\} \times e^{\pm i(h_1+h_2)t/2}, \tag{2.23}$$

which is recognized as the exact propagator of a coupled two-level system (i.e., for $h_n = \mathrm{const.}$). For vibronically coupled systems [i.e., for $h_n = h_n(x,p)$], Eq. (2.23) represents a short-time propagator which is exact in first order.

Now, the time integration in Eq. (2.13) can be performed easily. Accounting separately for the $e^{i\omega t}$ and the $e^{-i\omega t}$ part of the electric field, we readily obtain

$$P_{\pm} = \frac{1}{4}\mu e^{-\alpha\tau^2(\omega-2W)^2}\frac{\Delta}{W}\left\{\frac{V}{W}\sigma_z + \frac{\Delta}{W}\sigma_x \mp i\sigma_y\right\} + \frac{1}{2}\mu e^{-\alpha\tau^2\omega^2}\frac{V}{W}\left\{\frac{V}{W}\sigma_x - \frac{\Delta}{W}\sigma_z\right\}. \tag{2.24}$$

Within the rotating-wave approximation, the operators $P_+ \equiv A$ and $P_- \equiv E$ describe the absorption and the emission of a photon, respectively. Since both processes may occur in the case of internal transitions, the measured spectroscopic signal is given as the difference between absorption and emission signals[27]

$$I(t) = \langle\Psi_0(t)|(E^{\dagger}E - A^{\dagger}A)|\Psi_0(t)\rangle, \tag{2.25}$$

with

$$E^{\dagger}E-A^{\dagger}A=-\frac{1}{4}\mu^2 e^{-2\alpha\tau^2(\omega-2W)^2}\frac{\Delta^2}{W^2}\left\{\frac{\Delta}{W}\sigma_z-\frac{V}{W}\sigma_x\right\}$$
$$-\frac{1}{2}\mu^2 e^{-\alpha\tau^2[(\omega-2W)^2+\omega^2]}$$
$$\times\frac{V\Delta}{W^2}\left\{\frac{V}{W}\sigma_z+\frac{\Delta}{W}\sigma_x\right\}. \tag{2.26}$$

The first term exhibits the resonance condition $\omega=2W=W_2-W_1$, whereas the second term is off-resonant due to the $e^{-\alpha\tau^2\omega^2}$ term. In the limiting case of an impulsive probe pulse ($\tau=0$), the Gaussian resonance factors vanish and both terms may contribute. In the absence of vibronic coupling ($V=0$), Eq. (2.26) reduces to the well-known result $-\frac{1}{4}\mu^2 e^{-2\alpha\tau^2(\omega-2\Delta)^2}\sigma_z$.[10–16]

For interpretative purposes, it is instructive to change from the diabatic to the adiabatic electronic representation by using $P^{\mathrm{ad}}=S^{\dagger}PS$. This leads to the following expressions for the adiabatic absorption and emission propagators:

$$A_{\mathrm{ad}}=-\frac{1}{2}\mu\left\{\frac{\Delta}{W}e^{-\alpha\tau^2(\omega-2W)^2}|\psi_2^{\mathrm{ad}}\rangle\langle\psi_1^{\mathrm{ad}}|\right.$$
$$\left.+\frac{V}{W}e^{-\alpha\tau^2\omega^2}(|\psi_1^{\mathrm{ad}}\rangle\langle\psi_1^{\mathrm{ad}}|-|\psi_2^{\mathrm{ad}}\rangle\langle\psi_2^{\mathrm{ad}}|)\right\}, \tag{2.27}$$

$$E_{\mathrm{ad}}=-\frac{1}{2}\mu\left\{\frac{\Delta}{W}e^{-\alpha\tau^2(\omega-2W)^2}|\psi_1^{\mathrm{ad}}\rangle\langle\psi_2^{\mathrm{ad}}|\right.$$
$$\left.+\frac{V}{W}e^{-\alpha\tau^2\omega^2}(|\psi_1^{\mathrm{ad}}\rangle\langle\psi_1^{\mathrm{ad}}|-|\psi_2^{\mathrm{ad}}\rangle\langle\psi_2^{\mathrm{ad}}|)\right\}. \tag{2.28}$$

As in the diabatic case, there are two contributions. The first terms describe the laser-induced population transfer between the two adiabatic states, reflecting absorption in Eq. (2.27) and emission in Eq. (2.28). These transitions are seen to become resonant if the laser frequency ω matches the adiabatic electronic energy gap $2W=W_2(x)-W_1(x)$. A further coordinate dependency arises from the prefactor Δ/W, which represents the relation between the diabatic and the adiabatic energy gap. The second terms, on the other hand, affect a laser-induced level shift of the adiabatic electronic states which is proportional to $\mu V/W$. Being off-resonant and also vanishing in the absence of vibronic coupling, these terms may be omitted in all cases of interest. Neglecting the off-resonant terms, we finally obtain the simple result

$$E_{\mathrm{ad}}^{\dagger}E_{\mathrm{ad}}-A_{\mathrm{ad}}^{\dagger}A_{\mathrm{ad}}=\frac{1}{4}\mu^2\frac{\Delta^2}{W^2}e^{-2\alpha\tau^2(\omega-2W)^2}$$
$$\times(|\psi_2^{\mathrm{ad}}\rangle\langle\psi_2^{\mathrm{ad}}|-|\psi_1^{\mathrm{ad}}\rangle\langle\psi_1^{\mathrm{ad}}|), \tag{2.29}$$

i.e., in the case of internal coupling the light field induces *adiabatic* transitions.[28]

Let us finally consider the interpretation of the ubiquitous prefactors Δ/W and V/W. First note that these terms are directly connected with the diabatic/adiabatic mixing angle φ, i.e., $\Delta/W=\cos 2\varphi$ and $V/W=\sin 2\varphi$.[20] Hence, both terms assume values between -1 and 1, and satisfy the condition $(\Delta/W)^2+(V/W)^2=1$. Furthermore, it is interesting to notice that the transition dipole operator in the *adiabatic* representation $\hat{\mu}_{\mathrm{ad}}=S^{\dagger}\hat{\mu}S$ is given by

$$\hat{\mu}_{\mathrm{ad}}=\mu\frac{\Delta}{W}(|\psi_1^{\mathrm{ad}}\rangle\langle\psi_2^{\mathrm{ad}}|+|\psi_2^{\mathrm{ad}}\rangle\langle\psi_1^{\mathrm{ad}}|)$$
$$-\mu\frac{V}{W}(|\psi_1^{\mathrm{ad}}\rangle\langle\psi_1^{\mathrm{ad}}|-|\psi_2^{\mathrm{ad}}\rangle\langle\psi_2^{\mathrm{ad}}|), \tag{2.30}$$

thus clearly reflecting the structure of Eqs. (2.27) and (2.28).

C. External transitions

In the external case, one considers radiative transitions from the coupled states $|\psi_1\rangle$, $|\psi_2\rangle$ to one (or several) additional ''detector state(s)'' $|\psi_d\rangle$. Radiative $|\psi_1\rangle\leftrightarrow|\psi_2\rangle$ transitions between the coupled states $|\psi_1\rangle$, $|\psi_2\rangle$ are assumed to be dipole forbidden. The corresponding molecular Hamiltonian and transition dipole operator reads

$$H=\sum_{n=1,2,d}|\psi_n\rangle h_n\langle\psi_n|+\{|\psi_1\rangle V\langle\psi_2|+\mathrm{h.c.}\}, \tag{2.31}$$

$$\hat{\mu}=\sum_{n=1,2}|\psi_d\rangle\mu_{dn}\langle\psi_n|+\mathrm{h.c.} \tag{2.32}$$

In the following, we specialize to the case $\mu_{d1}=0$; that is, only a single electronic transition ($|\psi_2\rangle\leftrightarrow|\psi_d\rangle$) is dipole allowed. The more general case that both transition dipole moments are nonzero is treated in the Appendix.

The block structure of Hamiltonian (2.31) allows for a direct exponentiation of iHt within the semiclassical Franck–Condon approximation (2.18). The generalization of Eq. (2.23) to the three-state model reads

$$e^{\pm iHt}=e^{\pm ith_d}|\psi_d\rangle\langle\psi_d|+e^{\pm i(h_1+h_2)t/2}$$
$$\times\left\{\cos(Wt)\mathbb{1}\mp i\sin(Wt)\left(\frac{\Delta}{W}\sigma_z-\frac{V}{W}\sigma_x\right)\right\}, \tag{2.33}$$

where again Pauli matrices have been employed to conveniently represent the subspace of the diabatic coupled two-state system. This result is used to derive the corresponding Heisenberg transition dipole operator

$$\hat{\mu}(t)=e^{-itH}\hat{\mu}e^{itH}=\sum_{n=1,2}|\psi_d\rangle M_{dn}(t)\langle\psi_n|+\mathrm{h.c.}, \tag{2.34}$$

where

$$M_{d1}(t)=\mu e^{i\delta t}i\frac{V}{W}\sin(Wt), \tag{2.35a}$$

$$M_{d2}(t)=\mu e^{i\delta t}\left\{\cos(Wt)+i\frac{\Delta}{W}\sin(Wt)\right\}, \tag{2.35b}$$

and $\delta:=\frac{1}{2}(V_1+V_2)-V_d$.

Let us now assume that the detector state $|\psi_d\rangle$ is lower in energy than the two coupled electronic states $|\psi_1\rangle,|\psi_2\rangle$; i.e., we want to calculate the laser-induced emission from the

states $|\psi_1\rangle,|\psi_2\rangle$ into $|\psi_d\rangle$. In direct analogy to the derivation above, the corresponding emission projector P can be evaluated, thus yielding for $P^\dagger P/(\mu/4)^2)$ the expression

$$
\begin{aligned}
& e^{-2\alpha\tau^2[\omega-(W_2-V_d)]^2}\left(1+\frac{\Delta}{W}\right)\left(\mathbb{1}-\frac{\Delta}{W}\sigma_z+\frac{V}{W}\sigma_x\right) \\
& \quad + e^{-2\alpha\tau^2[\omega-(W_1-V_d)]^2}\left(1-\frac{\Delta}{W}\right)\left(\mathbb{1}+\frac{\Delta}{W}\sigma_z-\frac{V}{W}\sigma_x\right) \\
& \quad - 2e^{-\alpha\tau^2([\omega-(W_2-V_d)]^2+[\omega-(W_1-V_d)]^2)} \\
& \quad \times\frac{V}{W}\left(\frac{V}{W}\sigma_z+\frac{\Delta}{W}\sigma_x\right). \qquad (2.36)
\end{aligned}
$$

Considering a higher-lying detector state $|\psi_d\rangle$, the corresponding expression for excited-state absorption is readily obtained by changing the resonance terms (W_n-V_d) to (V_d-W_n). In the limiting case of an impulsive probe pulse $(\tau=0)$, the Gaussian resonance factors vanish and we obtain the simple result

$$P^\dagger P=\tfrac{1}{4}\mu^2|\psi_2\rangle\langle\psi_2|, \qquad (2.37)$$

i.e., in the impulsive limit the *diabatic* electronic population probability $\langle\Psi(t)|\psi_2\rangle\langle\psi_2|\Psi(t)\rangle$ is measured.[19,22,28]

In the case of finite probe pulses, the interpretation again becomes clearer by transforming Eq. (2.36) to the adiabatic representation. Here, the time-dependent transition dipole operator reads

$$\hat{\mu}_{\rm ad}(t)=S^\dagger\hat{\mu}S=\sum_{n=1,2}|\psi_d^{\rm ad}\rangle M_{dn}^{\rm ad}(t)\langle\psi_n^{\rm ad}|+{\rm h.c.}, \qquad (2.38)$$

$$M_{d1}^{\rm ad}(t)=-\mu\sqrt{\frac{1}{2}\left(1-\frac{\Delta}{W}\right)}\,e^{i(W_1-V_d)t}, \qquad (2.39a)$$

$$M_{d2}^{\rm ad}(t)=\mu\sqrt{\frac{1}{2}\left(1+\frac{\Delta}{W}\right)}e^{i(W_2-V_d)t}, \qquad (2.39b)$$

and we obtain

$$
\begin{aligned}
P_{\rm ad}^\dagger P_{\rm ad}=\frac{1}{8}\mu^2\Bigg\{ & e^{-2\alpha\tau^2[\omega-(W_2-V_d)]^2}\left(1+\frac{\Delta}{W}\right)|\psi_2^{\rm ad}\rangle\langle\psi_2^{\rm ad}| \\
& + e^{-2\alpha\tau^2[\omega-(W_1-V_d)]^2}\left(1-\frac{\Delta}{W}\right)|\psi_1^{\rm ad}\rangle\langle\psi_1^{\rm ad}| \\
& - e^{-\alpha\tau^2[[\omega-(W_2-V_d)]^2+[\omega-(W_1-V_d)]^2]} \\
& \times\frac{V}{W}(|\psi_1^{\rm ad}\rangle\langle\psi_2^{\rm ad}|+{\rm h.c.})\Bigg\}. \qquad (2.40)
\end{aligned}
$$

The first two terms account for the laser-induced emission from the states $|\psi_1\rangle$ and $|\psi_2\rangle$ into $|\psi_d\rangle$, respectively. These transitions become resonant, if the laser frequency ω matches the adiabatic energy gap W_n-V_d between these states. Containing both resonance conditions, the last term in Eq. (2.40) is usually strongly suppressed and can again be omitted in practice. Note that in the absence of vibronic coupling $(V=0)$, only the first term survives, since we have assumed that $\mu_{01}=0$. Recalling that the prefactors $(1\pm\Delta/W)$ represent the transformation matrix elements S_{nm} defined in Eq. (2.5), we obtain

$$
\begin{aligned}
P_{\rm ad}^\dagger P_{\rm ad}= & \tfrac{1}{4}\mu^2\sum_{n,m=1,2}S_{2n}|\psi_n^{\rm ad}\rangle\langle\psi_m^{\rm ad}|S_{2m} \\
& \times e^{-\alpha\tau^2[\omega-(W_n-V_d)]^2}e^{-\alpha\tau^2[\omega-(W_m-V_d)]^2}. \qquad (2.41)
\end{aligned}
$$

Neglecting furthermore the off-resonant terms, this result simplifies to

$$P_{\rm ad}^\dagger P_{\rm ad}=\tfrac{1}{4}\mu^2\sum_{n=1,2}e^{-2\alpha\tau^2[\omega-(W_n-V_d)]^2}S_{2n}^2|\psi_n^{\rm ad}\rangle\langle\psi_n^{\rm ad}|. \qquad (2.42)$$

Let us finally consider the case of ionization detection, whose calculation is particularly advantageous within the approximate description. Since ionization formally corresponds to an external absorption process into an ionic state $|\psi_I^{(k)}\rangle$ [cf. Eq. (2.9)], we may directly employ the formalism developed above to calculate time-resolved photoelectron spectra (2.15). Hence the electron continuum need not be discretized, but solely appears in the Gaussian resonance factors, which now read

$$\exp\{-2\alpha\tau^2[\omega-(E_k+\tilde{V}_I-W_n)]^2\}, \qquad (2.43)$$

i.e., to be resonant, a photon with frequency ω must provide the energy between the adiabatic state $|\psi_n^{\rm ad}\rangle$ and the ionic state $|\psi_I^{(k)}\rangle$ as well as the electron energy E_k. In order to directly calculate the total ionization probability (2.16), we need to integrate over E_k and Eq. (2.43) is replaced by

$$\sqrt{\frac{\pi}{8\alpha}}\frac{1}{\tau}\left[1+{\rm erf}\left(\frac{\omega-[\tilde{V}_I-W_n]}{\sqrt{2\alpha}\tau}\right)\right], \qquad (2.44)$$

where ${\rm erf}(x)=2\pi^{-1/2}\int_0^x e^{-t^2}\,{\rm d}t$ denotes the error function.

Since in principle any neutral electronic state can be ionized, we have to include radiative transitions from both coupled states $|\psi_1\rangle,|\psi_2\rangle$. For the two-state system under consideration, the two simplest cases of selection rules are that (i) both states ionize in one continuum, and (ii) each state ionizes in different continua. The first case is treated in the Appendix [cf. Eq. (A5)]. Assuming that the $|\psi_1\rangle\rightarrow|\psi_1^{(k)}\rangle$ and $|\psi_2\rangle\rightarrow|\psi_2^{(k)}\rangle$ transitions are allowed and neglecting off-resonant terms, the latter case is obtained as a direct extension of (2.42)

$$
\begin{aligned}
P_{\rm ad}^\dagger P_{\rm ad}= & \tfrac{1}{4}\sum_{n,m=1,2}\mu_{nn}^2e^{-2\alpha\tau^2[\omega-(E_k+\tilde{V}_n-W_m)]^2} \\
& \times S_{nm}^2|\psi_m^{\rm ad}\rangle\langle\psi_m^{\rm ad}|. \qquad (2.45)
\end{aligned}
$$

Compared to Eq. (A5) describing the case (i), Eq. (2.45) misses the interference terms.

III. COMPUTATIONAL EXAMPLES

A. Computational details

The computational methods employed for the numerical wave-packet propagations have been described in detail in Ref. 19. In short, the time-dependent Schrödinger equation is converted into a numerically tractable problem by expanding the state vector in a direct-product basis constructed from diabatic electronic states, free-rotor states for the torsional degree of freedom, and harmonic-oscillator states for the remaining vibrational degrees of freedom. This results in a system of coupled first-order differential equations, which are solved using a Runge–Kutta–Merson scheme with adaptive step size.

The spectroscopic signals (2.14) and (2.15) have been calculated (numerically) exactly as well as within the semiclassical Franck–Condon approximation. In the latter case, the spectroscopic signals are obtained as expectation values of the corresponding probe–pulse propagators $P^{\dagger}P$. This is done by transforming the time-dependent state vector to a grid in position space, whereby we employ the fact that the transformation matrix factorizes in a direct product of matrices depending only on a single vibrational mode.[21] The exact reference data have been obtained by a recently proposed method, which aims to combine the virtues of a perturbative description of the field–matter interaction with the advantages of a nonperturbative approach.[29] The concept of the method is to first evaluate the nonlinear electronic polarization for idealized δ-function pulses through a nonperturbative wave-packet propagation. Subsequently, the spectroscopic signals for finite pulses are calculated via convolution techniques stemming from perturbation theory. The exact reference data for the ionization calculations have been taken from Ref. 23.

B. Nonadiabatic photoisomerization

As a representative example for the case of *internal* radiative coupling, we consider a two-state three-mode model describing nonadiabatic *cis–trans* photoisomerization.[24,30] The model comprises a reaction coordinate along which the molecule undergoes isomerization (the ''torsional mode'' ϕ), a vibronically active mode which couples the electronic ground state and the excited state (the ''coupling mode'' x_c), and a totally symmetric mode which modulates the energy gap of the interacting states (the ''tuning mode'' x_t). The diagonal potential matrix elements of the diabatic model Hamiltonian (2.1) read

$$V_n = \sum_{j=t,c} \tfrac{1}{2}\omega_j x_j^2 + \kappa^{(n)} x_t + V^{(n)}(\phi), \tag{3.1}$$

where ω_j denotes the frequency of the jth vibrational mode and $\kappa^{(n)}$ represents the gradient of the excited-state potential-energy surface along the tuning mode. The off-diagonal diabatic coupling is given by $V_{12}=V_{21}=\lambda x_c$. The chemical aspects of the model are reflected by the torsional potentials

$$V^{(n)}(\phi) = E_n \pm \tfrac{1}{2} U_n (1-\cos\phi), \tag{3.2}$$

which are drawn in Fig. 1(a). Note that the excited-state potential $V^{(2)}(\phi)$ is inverted, i.e., the upper diabatic electronic state for $\phi=0$ (*cis* configuration) becomes the lower one for $\phi=\pi$ (*trans* configuration). The corresponding adiabatic potential-energy surfaces of the model system exhibit a conical intersection, which has been shown to trigger irreversible isomerization and internal-conversion dynamics on a femtosecond time scale.[19,30] Furthermore, various simulations of time- and frequency-resolved experiments have been reported for this model, thus demonstrating the possibility of a real-time observation of this elementary photochemical reaction.[24,31] Details on the model, the relaxation dynamics, and its time-resolved spectroscopy can be found in Refs. 19,24,30.

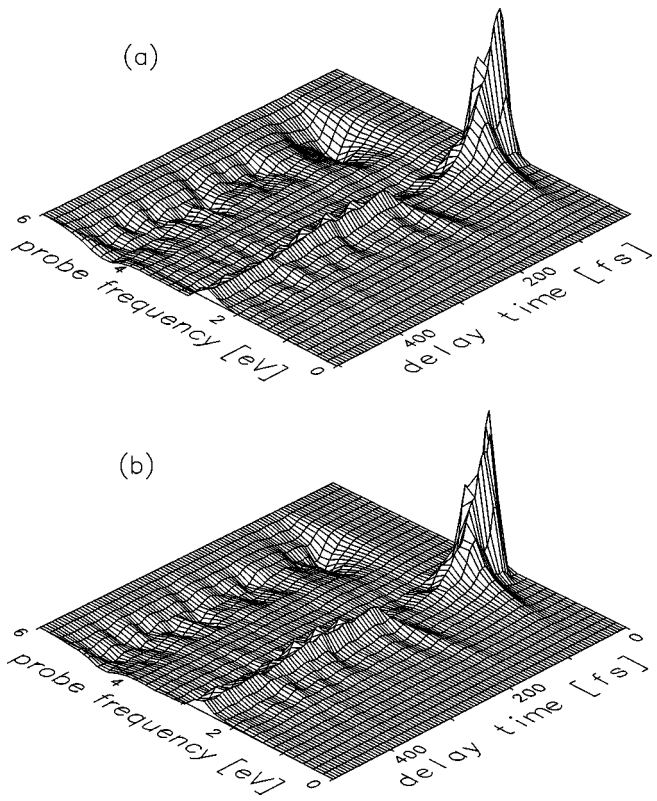

FIG. 2. Time- and frequency-resolved pump–probe spectrum of a two-state three-mode model system exhibiting nonadiabatic photoisomerization. The spectrum has been calculated (a) exactly, and (b) within the semiclassical Franck–Condon approximation. The calculation assumes impulsive excitation and Gaussian probe pulses of 10 fs duration.

To illustrate the ultrafast photoisomerization dynamics exhibited by the model, Fig. 2(a) shows an overview spectrum of the internal absorption and emission which has been drawn as a function of the delay time and the carrier frequency of the probe pulse. In the simulation we have assumed an impulsive pump pulse and a Gaussian probe pulse of duration $\tau=10$ fs. The ultrafast initial decay of the signal monitors the rapid delocalization of the wave packet on the excited electronic potential-energy surface. At time $t_d \approx 100$ fs, the wave packet has reached the conical intersection. This is reflected in a splitting of the pump–probe spectrum into two components, which correspond to the electronic gap of the system in the *cis* and *trans* configurations, respectively. The first component describes the stimulated emission of the reactants, while the latter describes the absorption of the pho-

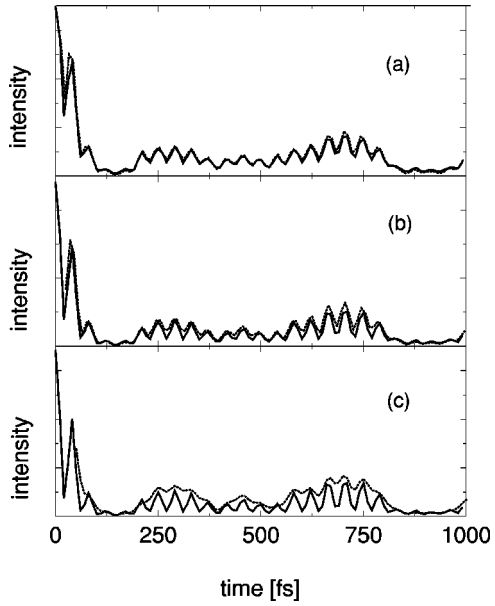

FIG. 3. Comparison of approximate (solid lines) and exact (dotted lines) pump–probe signals as obtained for the photoisomerization model at a laser frequency $\omega=2.75$ eV. The duration of the probe pulses is (a) $\tau=10$ fs, (b) $\tau=20$ fs, and (c) $\tau=40$ fs. The exact calculations are only shown for nonoverlapping laser pulses.

toproducts. A closer examination of the pump–probe signals reveals that both the absorption and the emission spectra exhibit quasiperiodic recurrences, thus reflecting coherent wave-packet motion in the ground- and excited electronic states.[24]

All the features of the exactly calculated spectrum Fig. 2(a) are seen to be nicely reproduced by the approximate calculation shown in Fig. 2(b). To investigate the accuracy of the approximation in more detail, Figs. 3 and 4 show representative cuts of the spectrum for the frequencies $\omega=2.75$ and 4.75 eV, respectively. Compared are approximate (solid lines) and exact (dotted lines) results for the probe pulse

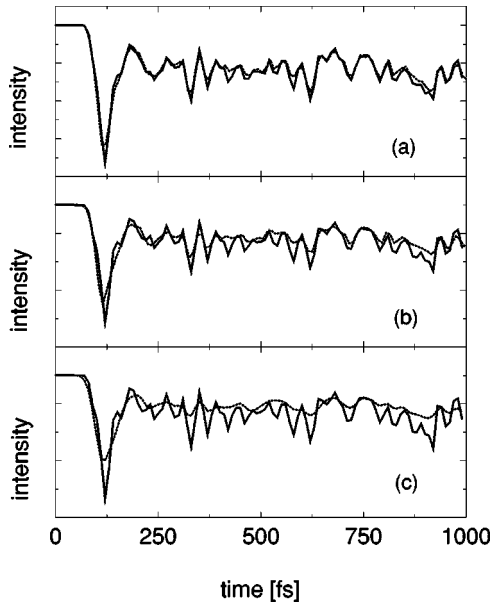

FIG. 4. Same as Fig. 3 except for $\omega=4.75$ eV.

durations (a) $\tau=10$ fs, (b) $\tau=20$ fs, and (c) $\tau=40$ fs.[32] As is expected, the approximation deteriorates with increasing pulse duration: While the agreement is excellent for 10 fs pulses and still very good for 20 fs pulses, the approximation only roughly matches the reference data for $\tau=40$ fs. In the latter case, spurious structures of the time-resolved signal indicate that the approximation fails to correctly account for the averaging effect caused by finite pulses. It is noted that the period of the fastest vibrational mode of the model is ≈ 40 fs. Neglecting the nuclear dynamics during the action of the laser pulse, the semiclassical Franck–Condon approximation (2.18) necessarily breaks down if the wave packet undergoes significant motion within the duration of the pulse.[10–12,16] The accuracy of the approximation is found to be roughly independent of the frequency chosen.

It should be noted, however, that the approximate scheme provides substantial computational savings in the case of multidimensional molecular systems. To generate the data for Fig. 2, for example, the approximate calculation requires about 50 times less CPU time than the exact method of Ref. 29.

Apart from computational advantages, the approximate expressions derived above may be used to facilitate the interpretation of time-resolved spectroscopy on nonadiabatically coupled molecular systems. As revealed by Eq. (2.29), in the internal case transitions between the coupled *adiabatic* electronic states are induced, which are enhanced by the resonance factor $e^{-2\alpha\tau^2(\omega-2W)^2}$. In the isomerization model under consideration there are two cases where this resonance condition can be met: In the *cis* configuration the adiabatic energy gap is $2W_{cis}=2.75$eV; in the *trans* configuration the adiabatic energy gap is $2W_{trans}=4.75$ eV. Tuning the laser to these resonances, Eq. (2.29) reveals that the pump–probe signal monitors the time-dependent probabilities

$$\mathcal{P}_{\rm ad}^{trans}(t)=\langle\Psi_0(t)|P_{trans}P_{\rm ad}|\Psi_0(t)\rangle, \tag{3.3}$$

$$\mathcal{P}_{\rm ad}^{cis}(t)=\langle\Psi_0(t)|P_{cis}P_{\rm ad}|\Psi_0(t)\rangle, \tag{3.4}$$

where $P_{\rm ad}=|\psi_2^{\rm ad}\rangle\langle\psi_2^{\rm ad}|-|\psi_1^{\rm ad}\rangle\langle\psi_1^{\rm ad}|$ and P_{cis} and P_{trans} denote the projector on the *cis* and *trans* configuration, respectively. This theoretical conclusion is reconfirmed by the numerical studies of Ref. 24.

C. $S_2\rightarrow S_1$ internal conversion in pyrazine

As a representative example for the case of *external* radiative coupling we consider a three-mode model of the $S_1(n\pi^*)$ and $S_2(\pi\pi^*)$ states of pyrazine.[26] Representing a standard example of ultrafast electronic relaxation, the model has given rise to a number of theoretical investigations, including exact[21,33] and approximate[34,35] studies of the time-dependent non-Born-Oppenheimer dynamics as well as simulations of cw[36] and time-resolved electronic spectra.[22,23] Including two tuning modes and a single coupling mode, the model reveals a low-lying conical intersection of the S_1 and S_2 states. The diabatic model Hamiltonian is given within the harmonic approximation, the parameters of the model can be found in Ref. 26.

To monitor in real time the $S_2\rightarrow S_1$ internal-conversion process in pyrazine, it has been suggested (i) to measure the

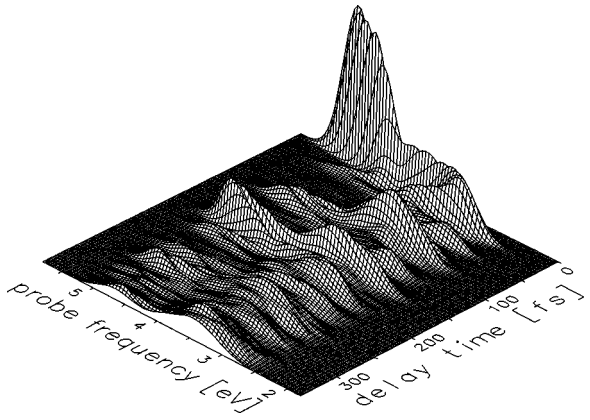

FIG. 5. Time- and frequency-resolved stimulated-emission pump–probe spectrum of a three-mode model of the $S_2 \rightarrow S_1$ internal-conversion process in pyrazine.

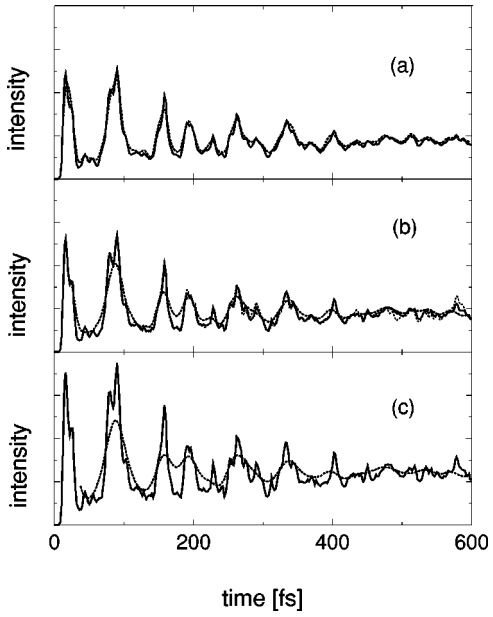

FIG. 6. Comparison of approximate (solid lines) and exact (dotted lines) pump–probe signals as obtained for the three-mode model of pyrazine at a laser frequency $\omega = 3.3$ eV. The duration of the probe pulses is (a) $\tau = 10$ fs, (b) $\tau = 20$ fs, and (c) $\tau = 30$ fs.

transient stimulated emission into the electronic ground state S_0,[22] and (ii) to ionize the molecule and record the time-resolved photoelectron spectrum.[23] In the first case, the selection rules are that the $S_2 - S_0$ transition is dipole allowed, the $S_2 - S_1$ transition is dipole forbidden, and the $S_0 - S_1$ transition is only weakly allowed and can be neglected to a good approximation. We therefore have the situation of a single external radiative transition ($S_2 \rightarrow S_0$) as described by Eq. (2.41). In the latter case, photoionization of the S_1 state leads to the ion-core ground state I_0, while ionization of the S_2 state leads to the first excited ion-core state I_1.[23] This corresponds to the situation of two external radiative transitions ($S_1 \rightarrow I_0$ and $S_2 \rightarrow I_1$) as described by Eq. (2.45).

Let us first consider the stimulated-emission pump–probe spectrum of the three-mode model of pyrazine. Assuming an impulsive pump pulse and 10 fs probe pulses, Fig. 5 shows a time- and frequency-resolved overview spectrum as obtained from evaluation of Eq. (2.36). Within only ≈ 20 fs the pump–probe signal undergoes a rapid initial decay which is accompanied by a significant redshift of the emission. For larger times, the spectrum is seen to bifurcate in two emission bands centered at the frequencies $\omega = 3.3$ and 4.8 eV. The time evolution of the emission exhibits pronounced recurrences, thereby reflecting vibrational wave-packet motion on coupled potential-energy surfaces.[22]

Since exact and approximate calculations of the overview spectrum are hard to distinguish for 10 fs pulses, we again consider cuts of the spectrum. Employing pulse durations of (a) 10 fs, (b) 20 fs, and (c) 30 fs, Figs. 6 and 7 compare exact and approximate calculations for the frequencies $\omega = 3.3$ and 4.8 eV, respectively. Similar to the discussion above, the approximation is excellent for 10 fs pulses and at least qualitatively correct for 20 fs pulses. Increasing the pulse duration to 30 fs, however, the approximation exhibits spurious structures and matches the reference calculation only roughly. This behavior is again directly correlated with the shortest vibrational period of the model $T \approx 32$ fs.

Let us employ the theory developed above to achieve an interpretation of the complex structures shown in Fig. 5. As off-resonant contributions can be omitted for the model considered, the spectrum can be explained by the simple expression (2.42), which is given as a sum ($n = 1,2$) over the products of resonance factors $e^{-2\alpha\tau^2[\omega-(W_n-V_d)]^2}$ and projectors $S_{2n}|\psi_n^{\mathrm{ad}}\rangle\langle\psi_n^{\mathrm{ad}}|S_{2n}$. From the resonance condition $\omega = W_n - V_d$ it is immediately clear that the two spectral bands at $\omega = 3.3$ and 4.8 eV can be identified as emission from the *adiabatic* S_1 and S_2 states, respectively. Employing resonant probe frequencies, the time evolution of the emission should therefore match the expectation value of the corresponding projector

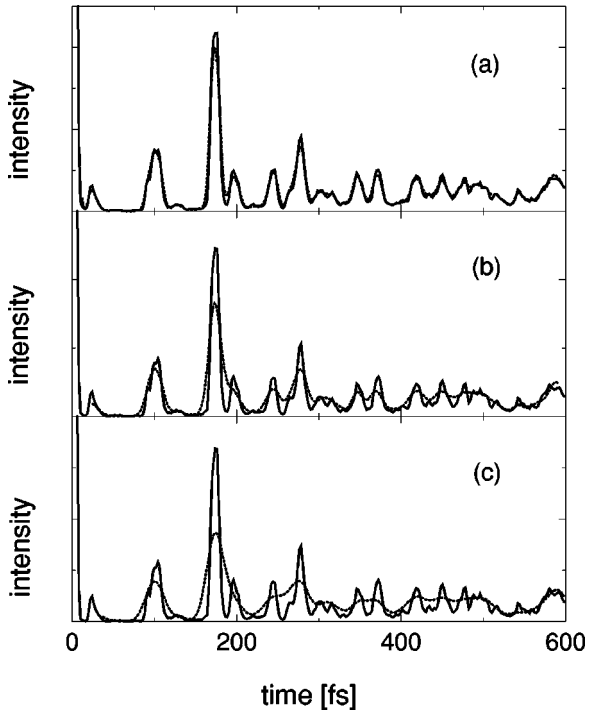

FIG. 7. Same as Fig. 6 except for $\omega = 4.8$ eV.

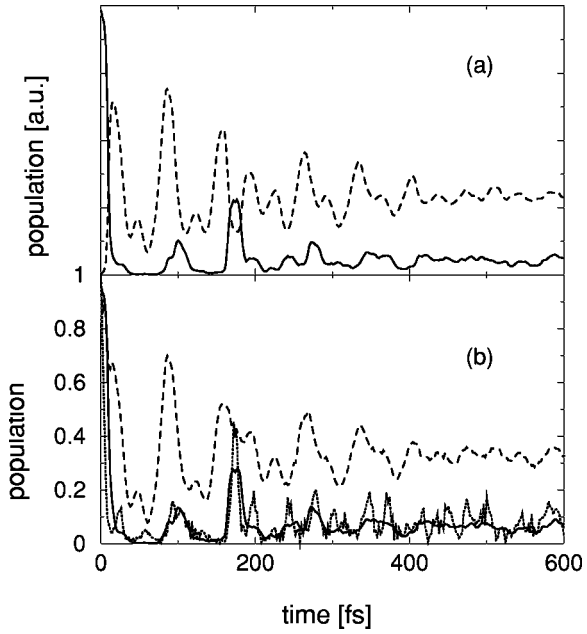

FIG. 8. Time-dependent observables reflecting the $S_2 \rightarrow S_1$ internal-conversion process of the pyrazine model. Shown are (a) the expectation values of the projectors $\mathcal{P}_1$ (dashed line) and $\mathcal{P}_2$ (solid line), (b) the squared modulus of the autocorrelation function (dotted line) and the population probability of the diabatic (dashed line) and adiabatic (solid line) upper electronic state, respectively.

$$\mathcal{P}_n(t) = \langle \Psi_0(t) | S_{2n} | \psi_n^{\mathrm{ad}} \rangle \langle \psi_n^{\mathrm{ad}} | S_{2n} | \Psi_0(t) \rangle, \tag{3.5}$$

whose time evolution is plotted in Fig. 8(a). While $\mathcal{P}_1(t)$ is indeed in good agreement with the pump–probe signal for $\omega = 3.3$ eV (cf. Fig. 6), the signal for $\omega = 4.8$ eV (cf. Fig. 7) is seen to exhibit more structure than $\mathcal{P}_2(t)$.

To explain these findings, it is helpful to introduce the population probability of the upper diabatic state $|\psi_2\rangle$, the upper adiabatic state $|\psi_2^{\mathrm{ad}}\rangle$, and the initial vibronic state $|\Psi_0(0)\rangle$

$$P_{\mathrm{di}}(t) = \langle \Psi_0(t) | \psi_2 \rangle \langle \psi_2 | \Psi_0(t) \rangle, \tag{3.6}$$

$$P_{\mathrm{ad}}(t) = \langle \Psi_0(t) | \psi_2^{\mathrm{ad}} \rangle \langle \psi_2^{\mathrm{ad}} | \Psi_0(t) \rangle, \tag{3.7}$$

$$C(t) = |\langle \Psi_0(t) | \Psi_0(0) \rangle|^2, \tag{3.8}$$

respectively, which are shown in Fig. 8(b). The importance of these time-dependent observables in the discussion of nonadiabatic excited-state processes has been studied in detail in Refs. 19–22, 28, and 33. In brief, the adiabatic population $P_{\mathrm{ad}}(t)$ decays within ≈ 20 fs and exhibits only minor recurrences thereafter. For larger times, $P_{\mathrm{ad}}(t)$ fluctuates around its long-time limit of 0.05, i.e., the system decays almost completely it its *adiabatic* ground state. The diabatic population $P_{\mathrm{di}}(t)$, on the other hand, is seen to exhibit an ultrafast initial decay which is followed by pronounced recurrences reflecting vibrational wave-packet motion. $C(t)$ is recognized as squared modulus of the electronic autocorrelation function, which qualitatively follows the adiabatic population dynamics.

A comparison reveals that $\mathcal{P}_2(t)$ closely reproduces the adiabatic population $P_{\mathrm{ad}}(t)$, whereas $\mathcal{P}_1(t)$ matches the diabatic population $P_{\mathrm{di}}(t)$ for times $\gtrsim 20$ fs. While the first result may be expected, it is an intriguing consequence of the almost complete depletion of the upper adiabatic state that the emission from the lower *adiabatic* state reflects the population dynamics of the upper *diabatic* state. The time-resolved emission stemming from the upper adiabatic state, on the other hand, is seen to recover the time evolution of the autocorrelation function $C(t)$. This is because for $\omega = 4.8$ eV the Gaussian resonance factor acts as a projector on the vibrational initial state.

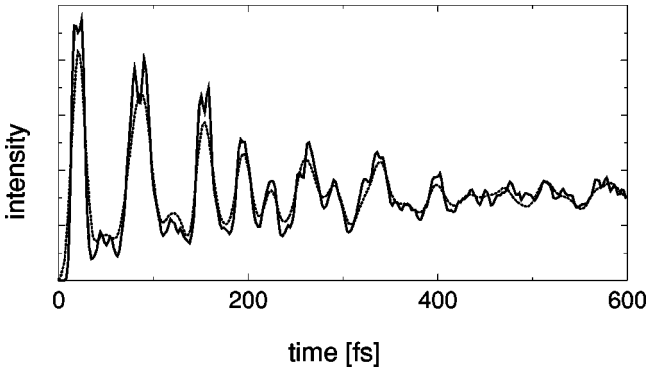

FIG. 9. Comparison of the approximate (solid lines) and exact [dotted lines (Ref. 23)] ionization signal of the pyrazine model monitored for an electron energy $E_k = 0.56$ eV and 16 fs pulses.

As an alternative mechanism to probe the nonadiabatic dynamics of the pyrazine model, we finally consider time-resolved ionization spectroscopy. As explained above, ionization formally corresponds to an external absorption process into an ionic state $|\psi_I^{(k)}\rangle$, where the index k refers to the kinetic energy E_k of the emitted electron [cf. Eq. (2.16)]. Due to this formal equivalence, the results obtained for the exact and approximate calculations of the photoelectron spectrum (2.15) are quite similar to the emission spectra discussed above. As a representative example, Fig. 9 shows a cut of the photoelectron spectrum as obtained for 16 fs probe pulses and $E_k = 0.56$ eV. At this energy of the photoelectrons, the probe laser is resonant to the $S_2 \rightarrow I_1$ transition and the photoelectron signal therefore monitors the diabatic population probability $P_{\mathrm{di}}(t)$. The quality of the approximation is similar to Fig. 6, although the onset of spurious structures can already be seen. It is interesting to compare these findings to the total ion yield $I_{\mathrm{Ion}}(t_d)$, which is obtained from the photoelectron spectrum $I_{\mathrm{Ion}}(t_d, E_k)$ via integration over E_k. Employing pulse durations of (a) 4 fs, (b) 16 fs, and (c) 32 fs, Fig. 10 compares exact and approximate calculations of $I_{\mathrm{Ion}}(t_d)$. Interestingly, the total ion yield is somewhat better reproduced by the approximation than in the case of the energy-resolved quantity $I_{\mathrm{Ion}}(t_d, E_k)$. As may be expected, the additional averaging employed in the calculation of $I_{\mathrm{Ion}}(t_d)$ helps to cancel errors of the approximation.

D. Effects of finite pump pulses

So far we have restricted ourselves to the case of impulsive excitation, that is, we have assumed a pump pulse whose duration is much shorter than any vibrational motion of the molecule. As a consequence, the prepared wave function $|\Psi_0(t)\rangle$ represents a coherent vibrational wave packet

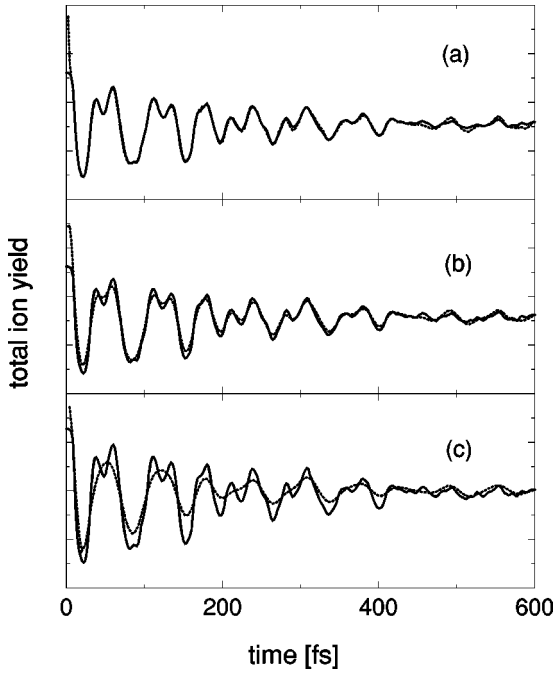

FIG. 10. Comparison of approximate (solid lines) and exact [dotted lines (Ref. 23)] total ionization yield as obtained for the three-mode model of pyrazine. The duration of the probe pulses is (a) $\tau=4$ fs, (b) $\tau=16$ fs, and (c) $\tau=32$ fs.

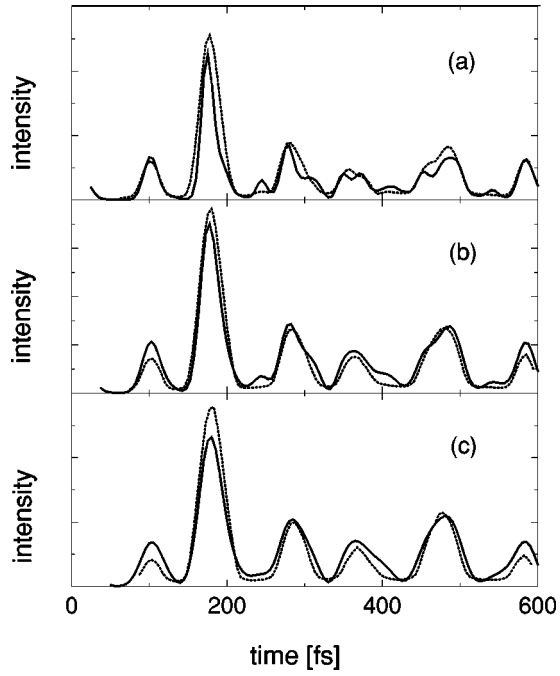

FIG. 11. Effects of finite pump pulses with durations (a) $\tau_{\mathrm{Pu}}=20$ fs, (b) $\tau_{\mathrm{Pu}}=30$ fs, and (c) $\tau_{\mathrm{Pu}}=40$ fs. Compared are approximate (solid lines) and exact (dotted lines) pump–probe signals as obtained for the three-mode model of pyrazine at a laser frequency $\omega=4.8$ eV.

which may give rise to oscillatory pump–probe signals. Employing pump pulses whose duration is longer than the vibrational time scales of the system, on the other hand, no coherent wave-packet motion may be induced and the coherent transients of the time-resolved signals vanish.

In the case of impulsive excitation, the Franck–Condon approximation was found to be valid if the vibrational motion during the action of the probe pulse can be neglected. In the following we wish to investigate to what extent finite pump pulses may affect the applicability of the approximation. Hereby the interaction with the pump pulse is treated exactly, while the Franck–Condon approximation is applied to the interaction of the system with the probe laser.[37] We restrict ourselves to the case of nonoverlapping laser fields. This restriction can readily be relaxed if one assumes that during the time the pulses coincide the interaction of the system with the pump pulse always comes before its interaction with the probe pulse. This is true, for example, in a two-color experiment, where the pump and probe laser excites different transitions, respectively.

As a representative example we again consider the stimulated-emission pump–probe signal of the three-mode model of pyrazine. Assuming impulsive excitation, it has been shown in Figs. 6 and 7 that the Franck–Condon approximation deteriorates considerably when the duration of the probe pulses approaches the period ($T\approx 32$ fs) of the fastest vibrational mode of the model. Assuming resonant ($\omega_{\mathrm{Pu}}=4.8$eV) pump laser pulses of the duration (a) $\tau_{\mathrm{Pu}}=20$ fs, (b) $\tau_{\mathrm{Pu}}=30$ fs, and (c) $\tau_{\mathrm{Pu}}=40$ fs, respectively, Fig. 11 compares exact and approximate calculations for 30 fs probe pulses with frequency $\omega=4.8$ eV. Interestingly, the quality of the approximation is seen to improve considerably for finite pump pulses. In particular, the spurious high-frequent oscillations that dominated the impulsive signal [cf. Fig. 7(c)] are largely suppressed for 20 fs pump pulses and completely absent for 40 fs pulses. This indicates that the approximation is mainly sensitive to vibrational motion that has been coherently excited by the pump pulse.

On the other hand, it should be noted that there is still no perfect agreement, e.g., the relative height of the peaks is reproduced only qualitatively in Fig. 11. Similar calculations for other model systems have shown that finite pump pulses in general improve the quality of the Franck–Condon approximation by removing the spurious oscillations. The approximation may still yield only qualitative agreement when the probe pulses are long compared to the vibrational time scales of the system. This finding may be understood by considering the Baker–Hausdorff formula $e^A e^B = e^{A+B+1/2[A,B]+\cdots}$ and recalling that in our case the neglected commutator terms are proportional to the nuclear momenta p_j.[10] Although the time-dependent mean momenta $\langle p_j\rangle_t$ go to zero for pump pulses which are longer than the vibrational period, the expectation value of the exponential function $\langle e^{\alpha p_j}\rangle_t$ does not vanish in general. As a remedy to this problem, the first correction term of the Baker–Hausdorff expansion may be included.[12]

IV. CONCLUDING REMARKS

Generalizing the semiclassical Franck–Condon approximation to the case of nonadiabatically coupled electronic states, we have developed a theoretical description of femtosecond pump–probe spectroscopy including time-resolved absorption, emission, and photoelectron detection. Assuming

nonoverlapping laser pulses, the formulation describes the probe process in terms of a propagator which is evaluated within first-order perturbation theory. The spectroscopic signals are given as expectation values of the propagator with respect to the time-dependent excited-state wave function prepared by the pump pulse. Employing Gaussian probe pulses, we have derived explicit expressions for these propagators, which are given in terms of resonance factors and electronic projection operators. In all cases considered, we obtain resonance conditions of the type $\omega = W_n - W_m$, where W_n and W_m denote the adiabatic potential-energy surfaces of the electronic states which are coupled by the radiation field with frequency ω. The projection operators depend on whether one considers radiative transitions between two vibronically coupled states or from the coupled states to an additional detector state. In both cases, the formulation allows for a simple interpretation of the femtosecond spectroscopy of nonadiabatically coupled molecular systems, which is most clearly given in the adiabatic representation. Based on the general expressions for the time-dependent dipole operator [Eqs. (2.21) and (2.34)], it is straightforward to extend the formulation given in this paper to other nonlinear spectroscopic techniques.

To study the applicability and accuracy of the approximation, we have employed two model problems of nonadiabatic photodynamics: a three-dimensional model describing the nonadiabatic *cis–trans* isomerization of an electronic two-state system and a three-mode model of the $S_2 \rightarrow S_1$ internal conversion in pyrazine. Choosing probe–pulse durations shorter than the period of the fastest relevant vibrational mode of the molecular system, the approximate theory has been found to be in quantitative agreement with the exact reference calculations. It has been shown that an even longer probe pulse may be employed, if the system is excited by a pump pulse whose duration is longer than the vibrational period. This finding indicates that the approximation is mainly sensitive to vibrational motion that has been prepared coherently. As the approximation virtually reduces the costs of explicit pump–probe simulations to the costs of a standard time-dependent wave-packet propagation, the formulation cuts the computational effort considerably. Since the theory requires no explicit discretization of a continuum of electronic states, this is particularly true for the description of femtosecond time-resolved photoelectron spectroscopy, which recently has been proven very promising in the real-time detection of nonadiabatic photoreactions.[38,39]

ACKNOWLEDGMENTS

We thank Jeffrey Cina for sending us a preprint of Ref. 16 and Matthias Seel for providing us with numerical data of Ref. 23. This work has been supported by the Deutsche Forschungsgemeinschaft and the Fonds der Chemischen Industrie.

APPENDIX

The results of Section II C can be easily generalized to the case that both transitions $|\psi_1\rangle \leftrightarrow |\psi_d\rangle$ and $|\psi_2\rangle \leftrightarrow |\psi_d\rangle$ are dipole allowed, that is, both dipole moments μ_{d1} and μ_{d2} are nonzero. In this case, the matrix elements of the Heisenberg transition dipole operator (2.34) read

$$M_{d1}(t) = \mu_{d1}\, e^{i\delta t}\left\{ \cos(Wt) - i\frac{\Delta}{W}\sin(Wt) \right\} + \mu_{d2}\, e^{i\delta t} i\frac{V}{W}\sin(Wt), \tag{A1}$$

$$M_{d2}(t) = \mu_{d2}\, e^{i\delta t}\left\{ \cos(Wt) + i\frac{\Delta}{W}\sin(Wt) \right\} + \mu_{d1}\, e^{i\delta t} i\frac{V}{W}\sin(Wt). \tag{A2}$$

In direct analogy to the derivation above, we find for the projector in the diabatic representation

$$\begin{aligned} P^\dagger P = \frac{1}{16}\Bigg\{ & e^{-2\alpha\tau^2[\omega-(W_2-V_d)]^2}\left(\mu_{d1}^2\left[1-\frac{\Delta}{W}\right] + \mu_{d2}^2\left[1+\frac{\Delta}{W}\right] + 2\mu_{d1}\mu_{d2}\frac{V}{W}\right)\left(\mathbb{1} - \frac{\Delta}{W}\sigma_z + \frac{V}{W}\sigma_x\right) \\ & + e^{-2\alpha\tau^2[\omega-(W_1-V_d)]^2}\left(\mu_{d1}^2\left[1+\frac{\Delta}{W}\right] + \mu_{d2}^2\left[1-\frac{\Delta}{W}\right] - 2\mu_{d1}\mu_{d2}\frac{V}{W}\right)\left(\mathbb{1} + \frac{\Delta}{W}\sigma_z - \frac{V}{W}\sigma_x\right) \\ & + 2e^{-\alpha\tau^2[[\omega-(W_2-V_d)]^2+[\omega-(W_1-V_d)]^2]}\left([\mu_{d1}^2-\mu_{d2}^2]\frac{V}{W} + 2\mu_{d1}\mu_{d2}\frac{\Delta}{W}\right)\left(\frac{V}{W}\sigma_z + \frac{\Delta}{W}\sigma_x\right)\Bigg\}. \end{aligned} \tag{A3}$$

A better physical understanding is again obtained in the adiabatic representation

$$\begin{aligned} P_{\mathrm{ad}}^\dagger P_{\mathrm{ad}} = \frac{1}{8}\Bigg\{ & e^{-2\alpha\tau^2[\omega-(W_2-V_d)]^2}\left(\mu_{d1}^2\left[1-\frac{\Delta}{W}\right] + \mu_{d2}^2\left[1+\frac{\Delta}{W}\right] + 2\mu_{d1}\mu_{d2}\frac{V}{W}\right)|\psi_2^{\mathrm{ad}}\rangle\langle\psi_2^{\mathrm{ad}}| \\ & + e^{-2\alpha\tau^2[\omega-(W_1-V_d)]^2}\left(\mu_{d1}^2\left[1+\frac{\Delta}{W}\right] + \mu_{d2}^2\left[1-\frac{\Delta}{W}\right] - 2\mu_{d1}\mu_{d2}\frac{V}{W}\right)|\psi_1^{\mathrm{ad}}\rangle\langle\psi_1^{\mathrm{ad}}| \\ & + e^{-\alpha\tau^2[[\omega-(W_2-V_d)]^2+[\omega-(W_1-V_d)]^2]}\left([\mu_{d1}^2-\mu_{d2}^2]\frac{V}{W} + 2\mu_{d1}\mu_{d2}\frac{\Delta}{W}\right)(|\psi_1^{\mathrm{ad}}\rangle\langle\psi_2^{\mathrm{ad}}| + \mathrm{h.c.})\Bigg\}. \end{aligned} \tag{A4}$$

In the limiting case $\mu_{d1}=0$, Eq. (2.40) is retained.

It should be noted that in the case that both coupled states carry oscillator strength, the averaging over molecular orientations has to be taken into account explicitly when calculating spectroscopic signals.[40] Denoting this averaging by $\langle \ldots \rangle$ and again dropping off-resonant terms, we finally obtain

$$P_{\mathrm{ad}}^{\dagger}P_{\mathrm{ad}}=\frac{1}{4}\sum_{\substack{m,n=1,2\\ m\neq n}} e^{-2\alpha\tau^2[\omega-(W_n-V_d)]^2}\left|\psi_n^{\mathrm{ad}}\right\rangle\left\langle\psi_n^{\mathrm{ad}}\right| \times(\langle\mu_{dn}^2\rangle S_{nn}^2+\langle\mu_{dm}^2\rangle S_{mn}^2 +2\langle\mu_{md}\mu_{nd}\rangle S_{mn}S_{nn}). \tag{A5}$$

[1] S. Mukamel, *Principles of Nonlinear Optical Spectroscopy* (University Press, Oxford, 1995).
[2] R. J. Kubo, J. Phys. Soc. Jpn. **12**, 570 (1957).
[3] E. J. Heller, Acc. Chem. Res. **14**, 368 (1981).
[4] M. Lax, J. Chem. Phys. **20**, 1752 (1952).
[5] R. Schinke, *Photodissociation Dynamics* (University Press, Cambridge, 1993).
[6] S. Mukamel, J. Chem. Phys. **77**, 173 (1982); Phys. Rep. **93**, 1 (1982).
[7] A. H. Zewail, *Femtochemistry—Ultrafast Dynamics of the Chemical Bond* (World Scientific, Singapore, 1994).
[8] *Femtosecond Chemistry*, edited by J. Manz and L. Wöste (VCH, New York, 1995).
[9] *Ultrafast Phenomena XI*, edited by T. Elsaesser, J. G. Fujimoto, D. A. Wirsma, and W. Zinth (Springer, Heidelberg, 1998).
[10] M. Braun, C. Meier, and V. Engel, J. Chem. Phys. **103**, 7907 (1995).
[11] M. Braun, C. Meier, and V. Engel, J. Chem. Phys. **105**, 530 (1996).
[12] S. Meyer, C. Meier, and V. Engel, J. Chem. Phys. **108**, 7631 (1998).
[13] R. Zadoyan, Z. Li, C. C. Martens, and V. A. Apkarian, J. Chem. Phys. **101**, 6648 (1994).
[14] M. Sterling, R. Zadoyan, and V. A. Apkarian, J. Chem. Phys. **104**, 6497 (1996).
[15] L. W. Ungar and J. A. Cina, Adv. Chem. Phys. **100**, 171 (1997).
[16] Y.-C. Shen and J. A. Cina, J. Chem. Phys. **110**, 9793 (1999).
[17] J. Michl and V. Bonačić-Koutecký, *Electronic Aspects of Organic Photochemistry* (Wiley, New York, 1990).
[18] F. Bernardi, M. Olivucci, and M. A. Robb, Chem. Soc. Rev. **25**, 321 (1996).
[19] W. Domcke and G. Stock, Adv. Chem. Phys. **100**, 1 (1997).
[20] H. Köppel, W. Domcke, and L. S. Cederbaum, Adv. Chem. Phys. **57**, 59 (1984).
[21] U. Manthe and H. Köppel, J. Chem. Phys. **93**, 345,1658 (1990).
[22] G. Stock, R. Schneider, and W. Domcke, J. Chem. Phys. **90**, 7184 (1989); G. Stock and W. Domcke, Phys. Rev. A **45**, 3032 (1992); J. Phys. Chem. **97**, 12466 (1993).
[23] M. Seel and W. Domcke, J. Chem. Phys. **95**, 7806 (1991).
[24] L. Seidner, G. Stock, and W. Domcke, J. Chem. Phys. **103**, 3998 (1995).
[25] B. Reischl, R. de Vivie-Riedle, S. Rutz, and E. Schreiber, J. Chem. Phys. **104**, 8857 (1996).
[26] R. Schneider and W. Domcke, Chem. Phys. Lett. **150**, 235 (1988).
[27] The mixed terms $E^{\dagger}A$ and $A^{\dagger}E$ have been omitted since they vanish in standard pump–probe experiments, which average over the phase of the electric field.
[28] H.-D. Meyer and H. Köppel, J. Chem. Phys. **81**, 2605 (1984).
[29] S. Hahn and G. Stock, Chem. Phys. Lett. **296**, 137 (1998).
[30] L. Seidner and W. Domcke, Chem. Phys. **186**, 27 (1994).
[31] L. Seidner, G. Stock, and W. Domcke, Chem. Phys. Lett. **228**, 665 (1994).
[32] In all calculations, approximate and exact nonperturbative data have been scaled by multiplication with a constant factor, which was usually chosen such that the signals coincide at the maximal delay time.
[33] R. Schneider, W. Domcke, and H. Köppel, J. Chem. Phys. **92**, 1045 (1990).
[34] M. Durga Prasad, Chem. Phys. Lett. **194**, 27 (1992); G. S. Latha and M. D. Prasad, J. Chem. Phys. **105**, 2972 (1996).
[35] G. Stock, J. Chem. Phys. **103**, 2888 (1995); U. Müller and G. Stock, *ibid.* **107**, 6230 (1997); *ibid.* **111**, 77 (1999).
[36] G. Stock and W. Domcke, J. Chem. Phys. **93**, 5496 (1990); *ibid.* **103**, 6851 (1995).
[37] Unlike the probing of the system as a function of the delay time and probe frequency, the interaction with the pump pulse needs to be calculated only a single time. It is therefore not a time-consuming task and can be readily performed exactly. Within the Franck–Condon approximation, finite pump pulses and overlapping laser fields have been described in Ref. 16.
[38] D. R. Cyr and C. C. Hayden, J. Chem. Phys. **104**, 771 (1996).
[39] V. Blanchet, M. Z. Zgierski, T. Seideman, and A. Stolow, Nature (London) **401**, 52 (1999).
[40] R. Heather and H. Metiu, J. Chem. Phys. **90**, 6903 (1989).